Effect of Oxidation on the Structure of Human Low- and High-Density Lipoproteins

Cristiano L. P. Oliveira,* Priscila R. Santos, Andrea M. Monteiro, and Antonio M. Figueiredo Neto
Instituto de Física, Universidade de São Paulo, São Paulo, Brazil

ABSTRACT This work presents a controlled study of low-density lipoprotein (LDL) and high-density lipoprotein (HDL) structural changes due to in vitro oxidation with copper ions. The changes were studied by small-angle x-ray scattering (SAXS) and dynamic light scattering (DLS) techniques in the case of LDL and by SAXS, DLS, and Z-scan (ZS) techniques in the case of HDL. SAXS data were analyzed with a to our knowledge new deconvolution method. This method provides the electron density profile of the samples directly from the intensity scattering of the monomers. Results show that LDL particles oxidized for 18 h show significant structural changes when compared to nonoxidized particles. Changes were observed in the electrical density profile, in size polydispersity, and in the degree of flexibility of the APO-B protein on the particle. HDL optical results obtained with the ZS technique showed a decrease of the amplitude of the nonlinear optical signal as a function of oxidation time. In contrast to LDL results reported in the literature, the HDL ZS signal does not lead to a complete loss of nonlinear optical signal after 18 h of copper oxidation. Also, the SAXS results did not indicate significant structural changes due to oxidation of HDL particles, and DLS results showed that a small number of oligomers formed in the sample oxidized for 18 h. All experimental results for the HDL samples indicate that this lipoprotein is more resistant to the oxidation process than are LDL particles.

INTRODUCTION

Cholesterol is a hydrophobic molecule that is essential for the structure of the cell membrane and is a precursor of bile acids, vitamin D, and other steroids. Plasma lipoproteins are responsible for the transport of cholesterol between cells. These quasispherical particles of different size and composition are composed of a lipid core of triglycerides and cholesterol esters surrounded by a monolayer of phospholipids, free cholesterol, and apolipoproteins (Apo). Apolipoproteins are essential for the structural integrity of the particle in addition to controlling lipoprotein metabolism through binding to specific cell-membrane receptors (1,2). The low-density lipoprotein (LDL), responsible for the delivery of cholesterol to peripheral tissues, has only one apolipoprotein (ApoB, predominantly B-100) (3), whereas high-density lipoproteins (HDLs), which mediate the inverse process of cholesterol transport (4), contain several apolipoproteins (e.g., ApoA, C, and E) (5,6).

It is well established that lipoproteins play a key role in atherosclerosis. This illness is the leading cause of death in the western world. It is characterized as a dynamic and progressive inflammatory disease that promotes lipid deposition in the arteries that may result in the formation of atherosclerotic plaques in the intima of the vessel. Elevated (reduced) plasma levels of LDL (HDL) are associated with an increase of coronary artery disease (CAD) (7,8).

LDL particles can undergo a modification process due to the action of reactive oxygen species (ROS) and reactive nitrogen species (RNS). The oxidation of LDL is a complex process that begins with the peroxidation of some polyunsaturated fatty acids (PUFAs), mainly phospholipids and cholesteryl esters. Moreover, the oxidation products cause changes in the ApoB conformation and affect the functional properties of LDL (9). Structural and/or chemical changes generate different types of modified LDL particles (mLDL), of which one of the most common is oxidized LDL (oxLDL). OxLDL is removed by intima macrophages via scavenger receptors that are not downregulated, causing an excessive intracellular accumulation of LDL and foam-cell formation (10). This process characterizes the first phase of atheroma plaque formation. Studies show that in contrast, HDL may play an antiatherogenic and antithrombotic role (11) by protecting LDL against lipid peroxidation and reducing the deleterious effect of the oxLDL (12–14).

There are few methods to quantify the oxLDL in the plasma. Gomez et al. (15) developed a new method to determine the concentration of oxLDL by measuring the nonlinear optical response of LDL solutions. The Z-Scan (ZS) technique was used to investigate the nonlinear optical properties of native LDL and oxLDL. The higher the degree of oxidation of LDL particles, the smaller was the nonlinear optical signal. Applying the ZS technique, Monteiro et al. (16) showed that periodontitis patients have higher concentrations of modified LDL compared to individuals without periodontal disease. Moreover, periodontal treatment reduced the concentration of oxLDL in the plasma (17).

The use of small angle x-ray scattering (SAXS) to study the structure of HDL and LDL particles dates back to the 1970s. Laggner and co-workers suggested that HDL particles were spherical objects with an average diameter of 9.6 nm (18). That work and others of the same period presented the first electron density profiles of HDL and LDL particles obtained by SAXS measurements made using

Submitted February 24, 2014, and accepted for publication April 30, 2014.

*Correspondence: crislpo@if.usp.br

Editor: Lukas Tamm

0006-3495/14/06/2595/11 $2.00

http://dx.doi.org/10.1016/j.bpj.2014.04.049

simplified procedures, which were only capable of providing an overview of the internal structure of these lipoprotein particles. Scattering results also suggested that the LDL particles are spherical in shape, with an average diameter of 24 nm and a possible lamellar organization of the lipid core (19,20). Since these seminal works, methods for analyzing results obtained using the SAXS technique have evolved significantly. The deconvolution square-root procedure proposed by Glatter (21,22) has been applied in several studies of lipoproteins (23). Such studies represented important advances in understanding the structure of lipoproteins. For example, SAXS results for measurements of in vitro oxLDL particles showed no major structural changes in samples oxidized with copper for <25 h (23). Over the past 40 years, knowledge about lipoprotein structure has expanded considerably, but several questions about cholesterol packing in the inner region of LDL particles and the conformational orientation of apolipoproteins remain (24–26). Recent studies with cryomicroscopy point to a lamellar organization of cholesterol in the inner region of LDL particles and to the influence of triglycerides on the temperature at which the transition from this lamellar phase to a disorganized one occurs (27).

In this work, we investigate the structure of LDL and HDL particles using the SAXS technique and present to our knowledge a new approach for analysis of these data. This approach was originally developed by Oliveira and co-workers to model experimental curves of scattering intensity and obtain electron density profiles of lamellar systems (28). The model was adapted to systems with spherical symmetry so that it could be used for LDL and HDL SAXS data. The obtained fits of the experimental scattering curves are significantly better than those reported in the literature (19,20,23), producing more accurate and reliable curves for the electron density profile. The discussion of the results and analysis of the structural properties of the particles is complemented by dynamic light scattering (DLS) measurements and the nonlinear optical response of the particles. As this response has already been discussed in the literature for LDL particles, ZS experiments were performed with HDL solutions to get a complete set of data for both lipoproteins.

MATERIALS AND METHODS

Isolation and oxidation of LDL and HDL

Blood was drawn from healthy normolipidemic donors, and the plasma was obtained after centrifugation at 1000 × *g* at 4°C for 15 min. Benzamidine (2 mM), chloramphenicol (0.25%), phenylmethylsulfonyl fluoride (0.5 mM), gentamicin (0.5%), and aprotinin (0.1 U/mL) were added to the plasma. LDL (1.006 < d < 1.063 mg/dL) and HDL (1.063 < d < 1.21 mg/dL) were isolated by density difference in a sequential ultracentrifugation (29) process at $10^5 \times g$ at 4°C, using the rotor of an ultracentrifuge (Hitachi Ultracentrifuge, Tokyo, Japan). The obtained samples with LDL and HDL were dialyzed for 24 h at 4°C against phosphate-buffered saline (PBS), pH 7.4. The LDL and HDL were put through a filter with micrometer-sized pores (Millipore, Schwalbach, Germany), and the protein concentration was determined using a bicinchoninic acid protein assay kit (Pierce, Stowe, VT), with bovine serum albumin as standard.

In vitro oxLDL and oxHDL were obtained by incubation of native LDL (naLDL) and HDL (naHDL), respectively, with 20 μM $CuSO_4$/mg protein at 37°C (30). The samples were oxidized for 5, 30, and 60 min, 6 h, and 18 h (Table 1). At each predefined time, the oxidation reaction was inhibited with the addition of 1 mM of EDTA to the sample solution. After this procedure, HDL and LDL samples are ready to be used.

Z-scan

The ZS setup was composed of a continuous-wave Nd:YVO_4 ($\lambda = 532$ nm) Verdi V10 laser from Coherent (Santa Clara, CA), with a Gaussian profile beam. In this setup, the laser beam was chopped at 17 Hz and focused by a 25.4 mm lens with focal distance $f = 150$ mm, which gave a Rayleigh length of $z_0 = 3.84 \pm 0.20$ mm (31). In these conditions, the beam (consecutively) illuminates the sample during the time interval $\Delta t = 30$ ms. A silicon photodetector (PDA36A, THORLABS, Newton, NJ), positioned at the far field, collected the transmitted light. All HDL samples were investigated using glass sample holders 200 μm thick and 180 mW of incident power of the laser on the samples. In the ZS experiment, the sample is moved along the z axis, around the laser-beam focus position. The detector collects the transmitted light as a function of the z-position and time $I(z,t)$. At a given z-position the transmittance is recorded during the time $0 < t < \Delta t$. The z-dependence of the normalized transmittance, $\Gamma_N(z)$, is written as (31):

$$\Gamma_N(z) = \frac{I(z, t = 0) - I(z, t = \Delta t)}{I(z, t = \Delta t)} = \theta\left(\frac{2(z/z_0)}{1 + (z/z_0)^2}\right) + \theta^2\left(\frac{1}{1 + (z/z_0)^2}\right), \quad (1)$$

where θ is a dimensionless parameter that measures the strength of the thermal lens formed in the sample. The typical ZS-position-dependent curve has a peak and a valley. The peak to valley amplitude is proportional to the parameter θ. Thus, the bigger θ is, the larger is the peak-to-valley amplitude and, consequently, the thermal lens strength. Each measurement was repeated 10 times in 80 different z-positions around the beam waist. The data were analyzed using the Thermal Lens model (31). More details about the setup, data acquisition, and data treatment can be found in a previous work (32).

SAXS

LDL SAXS measurements were performed at the Brazilian Synchrotron Light Laboratory (LNLS) at the SAXS1 beamline (33). The sample holder, a cell with dimensions $1 \times 4 \times 8$ mm^3 and mica windows, was connected to a thermal bath, enabling LDL sample measurements with the temperature controlled at 22°C. The wavelength of the incoming monochromatic

TABLE 1 Descriptions of all lipoprotein samples

Sample	Description
naLDL	Native LDL
oxLDL-05min	LDL oxidized with Cu for 5 min
oxLDL-30min	LDL oxidized with Cu for 30 min
oxLDL-60min	LDL oxidized with Cu for 60 min
oxLDL-6h	LDL oxidized with Cu for 6 h
oxLDL-18h	LDL oxidized with Cu for 18 hours
naHDL	Native HDL
oxHDL-30min	HDL oxidized with Cu for 30 min
oxHDL-60min	HDL oxidized with Cu for 60 min
oxHDL-18h	HDL oxidized with Cu for 18 h

x-ray beam was $\lambda = 1.48$ Å, and the distance between the sample and the detector was set to 3200 mm, providing a q (scattering vector modulus) interval from 0.006 to 0.25 $Å^{-1}$, where $q = 4\pi(\sin\xi)/\lambda$ and 2ξ is the scattering angle. The 2D scattering data were collected on a Pilatus 300k detector (Dectris, Baden, Switzerland), and integration of the SAXS patterns and data treatment were performed using FIT2D software (34). Error estimation and normalization to absolute scale were performed with the SUPERSAXS package (C. L. P. Oliveira and J. S. Pedersen, unpublished). A beam size of 300×100 μm was used. This beam size is further convoluted with a detector resolution of 172 μm. The experimental setup provided a spacing in q values of $\Delta q = 0.00042 Å^{-1}$.

HDL SAXS measurements were performed on the laboratory SAXS instrument Nanostar (Bruker, Billerica, MA) at the Institute of Physics, University of São Paulo. This equipment is improved by the use of microfocus source Genix3D coupled with Fox3D multilayer optics and two sets of scatterless slits for beam definition, all provided by Xenocs (Sassenage, France). The samples were kept on a quartz capillary glued to a stainless-steel case, which facilitated proper rinse and reuse of the sample holder, permitting an accurate background subtraction. The scattering of water measured on the same sample holders was used to normalize the data to absolute scale. The sample temperature was controlled by a circulating bath and was kept constant at 25°C. Several 900 s frames were recorded for each sample to monitor radiation damage and beam stability. The wavelength of the incoming monochromatic x-ray beam was $\lambda = 1.54$ Å ($Cu_{k\alpha}$) and the sample-to-detector distance was 0.67 m, providing a q interval from 0.009 to 0.35 $Å^{-1}$. The 2D scattering data were collected on a Vantec2000 detector (Bruker), and integration of the SAXS patterns was performed using Bruker SAXS software. The data treatment, normalization to absolute scale, and averaging procedures were performed using the SUPERSAXS package (C. L. P. Oliveira and J. S. Pedersen, unpublished). A beam size of 1 mm in diameter was used. This beam size is further convoluted with a detector resolution of 160 μm. The experimental setup provided a q-value spacing of $\Delta q = 0.00142 Å^{-1}$.

The treated and normalized SAXS data for the sample series of LDL and HDL is shown in Fig. S1 in the Supporting Material.

SAXS data analysis and modeling

The analysis of the SAXS data was performed in several steps. First, the data were analyzed by the indirect Fourier transformation (IFT) method (35) in a slightly different implementation (36,37). The IFT fits for several data sets and the corresponding $p(r)$ functions are shown in Fig. S2, *a* and *b*. From these analyses, initial information about size, shape, and possible aggregation were obtained. For the LDL samples, it was observed that the presence of oligomers or larger aggregates depends on the level of oxidation. Interestingly, for the HDL samples, no aggregation was detected. To be able to analyze the contribution only from the LDL particles, not from the aggregates, it is necessary to decouple the form and structure factors of the scattering data. We were able to do so using the generalized IFT method (GIFT) (36). In this case, a theoretical function is used for the structure-factor contribution and it is possible, by simultaneous optimization of the $p(r)$ function (form-factor) and structure-factor parameters, to obtain the theoretical form factor without the structure-factor contribution. For the case of HDL, this decoupling procedure was not necessary.

Having the form factors for each case, a new analysis method was used. This procedure is based on the square-root deconvolution method originally proposed by Glatter (21,22), but with a different implementation, similar to that proposed by Oliveira (28). In the original method proposed by Glatter, modeling was performed by fitting the $p(r)$ curve. This approach limits the generality of the model, since only spherical (cylindrical and lamellar) systems could be studied, without the inclusion of any kind of anisotropy. In the proposed new method, since the scattering data are adjusted, it is possible to introduce several types of anisotropy, e.g., as polydispersity, as well as to perform a simultaneous fitting of additional backgrounds to the scattering data and several other types of contribution (28).

The description of the normalized intensity form factor ($P(q)$) and amplitude form factor ($A(q)$) is performed using an analytical or semianalytical expression that can be written as

$$P_{MOD}(q) = \frac{\int_0^\infty D(r)m(r)^2 P_{Mon}(q,r)dr}{\int_0^\infty D(r)m(r)^2 dr} \quad (2)$$

$$A_{MOD}(q) = \frac{\int_0^\infty D(r)m(r)^2 A_{Mon}(q,r)dr}{\int_0^\infty D(r)m(r)^2 dr}, \quad (3)$$

where a number distribution polydispersity in size was assumed. Several types of distribution, for example, Shulz-Zimm distributions, can be assumed. The function $m(r)$ depends on the assumed geometry. For spheroidal particles, $m(r) = V$, where V is the particle volume. Different geometries may have different weighting functions. The intensity and amplitude form factors, $P_{Mon}(q)$ and $A_{Mon}(q)$ for ellipsoidal particles are given by

$$P_{Mon}(q) = \int_0^{\pi/2} \left(F_M[q, r(R,\varepsilon,\alpha)] \exp\left[-\frac{1}{2} q^2 \sigma_{\text{int}} \right] \right)^2 \sin\alpha \, d\alpha \quad (4)$$

$$A_{Mon}(q) = \int_0^{\pi/2} F_M[q, r(R,\varepsilon,\alpha)] \exp\left[-\frac{1}{2} q^2 \sigma_{\text{int}} \right] \sin\alpha \, d\alpha, \quad (5)$$

where $r(R, \varepsilon, \alpha) = R(sin^2\alpha + \varepsilon\, cos^2\alpha)^{1/2}$ is the radial element for the integration, R is the transversal radius, and εR is the vertical radius of the ellipsoid of revolution. The Gaussian term on the formula provides a smearing of the interface.

The function $F_M(q,R)$ describes an ellipsoidal particle with several shells of different electron density (Fig. 1) and is given by

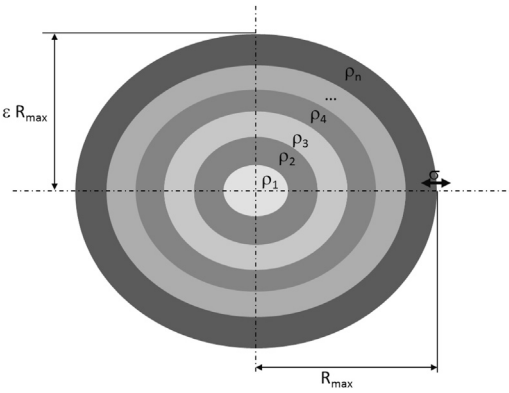

FIGURE 1 Schematic drawing of the model used to obtain the electron density profile of lipoproteins. $R_{\max}$ is the maximum radius of the particle and ε is its anisotropy. Thus, if $\varepsilon = 1$, the particle is spherical, if $\varepsilon < 1$, it is an oblate spheroid, and if $\varepsilon > 1$, the particle has the shape of a prolate spheroid.

$$F_M(q) = \frac{1}{M_M}\left[\rho_1 m(R_1)F_S(q,R_1) + \sum_{i=2}^{N}(\rho_i - \rho_{i-1})m(R_i)F_S(q,R_i)\right] \quad (6)$$

$$M_M = \rho_1 m(R_1) + \sum_{i=2}^{N} m(R_i)(\rho_i - \rho_{i-1}), \quad (7)$$

where ρ_i is the electron density for the ith layer, N is the number of shells/layers describing the model, and $F_S(q,R)$ is the amplitude form factor for a sphere of radius R:

$$F_S(q,R) = \frac{3[\sin(qR) - qR\cos(qR)]}{(qR)^3}. \quad (8)$$

The final expression used for fitting the theoretical data is

$$I(q) = S_{C_1}P_{MOD}(q) + S_{C_2}P_{Deb}(q) + Back. \quad (9)$$

In this expression, the form factor $P_{MOD}(q)$ is defined in Eq. 1, S_{C1} and S_{C2} are scale factors, *Back* is a constant background, and $P_{Deb}(q)$ is the intensity factor for the scattering from a Gaussian chain, given by

$$P_{Deb}(q) = 2[\exp(-u) + u - 1]/u^2, \quad (10)$$

where $u = Rg^2q^2$, where Rg is the average radius of gyration of the Gaussian chain. This expression was used to describe two general features of the lipoprotein systems that may directly affect the scattering data. The first is the presence of proteins on the surface of the lipoprotein (ApoB for LDL and several proteins for HDL), which introduce a break in symmetry in the system that naturally makes the form-factor minima shallower. Also, those proteins can have floppy or flexible regions that can also be described by Eq. 10.

In the results shown in this work, a total of $N = 10$ shells was considered in Eq. 6. The modeling parameters are the electron densities, ρ_i, of each shell; the maximum radius of the particle; the polydispersity in radius, assuming a Shulz-Zimm distribution; the particle anisotropy, ε (>1 for prolate and <1 for oblate); two scale factors, S_{C1} and S_{C2}, the radius of gyration of the Gaussian chain, and a constant background. All these parameters were optimized in the same fitting procedure. We used a nonlinear partially constrained least-squares fitting (28,38) in which the ρ_i values are stabilized by the use of a Lagrange multiplier that is varied during the fitting procedure. The best value of this Lagrange multiplier is automatically determined by the modeling procedure.

Dynamic light scattering (DLS)

The DLS technique was used to evaluate the particle-size distribution on the samples. LDL measurements were performed using a Zetasizer Nano ZS (Malvern, Worcestershire, United Kingdom) at the Institute of Chemistry, University of São Paulo. The experimental setup was composed of a 633 nm wavelength laser beam and a photon detector positioned at 7° (with respect to the detector). HDL measurements were performed using a 90Plus Particle Size Analyzer (Brookhaven, Holtsville, NY) located at the Institute of Physics, University of São Paulo. The setup was composed of a laser beam with wavelength 657 nm and a detector positioned at 90°. Temporal autocorrelation curves were obtained using standard routines of the acquisition programs. Through standard DLS models and the Contin method (39), we calculated the average diameter of monomers and clusters comprising the samples. The DLS experiment was performed in homodyne mode on both instruments.

RESULTS

SAXS results

Low-density lipoproteins

The analysis of LDL samples started with the use of the IFT method. The obtained pair distance distribution functions, ($p(r)$), for all samples showed a well-defined monomeric region and a second region that could be related to the presence of small oligomers in the samples (data shown only in Fig. S2, *a* and *b*). Decoupling of the monomer contribution (form factor) and the small-oligomer contribution (structure factor) was performed using the GIFT method (36). One example of fitting and its contributions is shown in Fig. 2. In this case, we used a structure factor of a fractal system (40). One can clearly see that this model is able to describe the full SAXS curve. It is easy to see that the form factor detaches from the experimental data for small q values, suggesting that this region of the scattering data is dominated by larger objects, the LDL oligomers, which are then described by the structure factor. The presence of such oligomers is supported both by IFT analysis of LDLs (Fig. S2 *b*) and by previous TEM studies (41). In all LDL samples, the clusters were best fitted as fractals, with fractal dimension compatible with 3.0, indicating that they were volume (3D) fractals. Since just a few points are related to the structure factor on the SAXS profile, the average size/correlation of such fractals (the so-called cutoff length on the model used (40)) was not well defined and varied between ~2000 and ~4000 Å. In any case, the modeling of such oligomers is an approximation and has to be viewed as a procedure to decouple the best form factor for this system.

The maximum appearing at $q = 0.17$ Å^{-1} in the experimental scattering data (Fig. 3 *a*), is related to the repetition distance of ~37 Å associated with a lamellar packing of the lipid content in the LDL core (27). The lamellae are composed of two bound molecules of cholesterol esters.

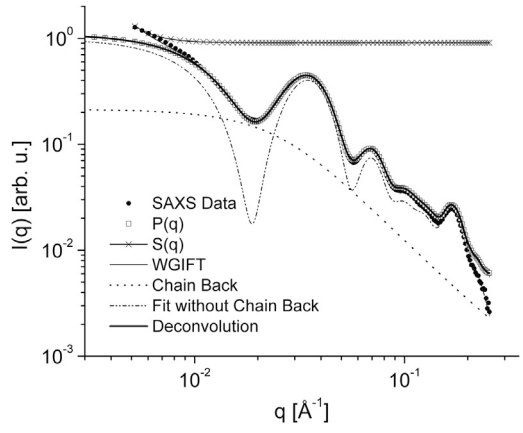

FIGURE 2 Example of data fitted with the GIFT and deconvolution methods, showing the contribution of each component in the fit. For details, see text.

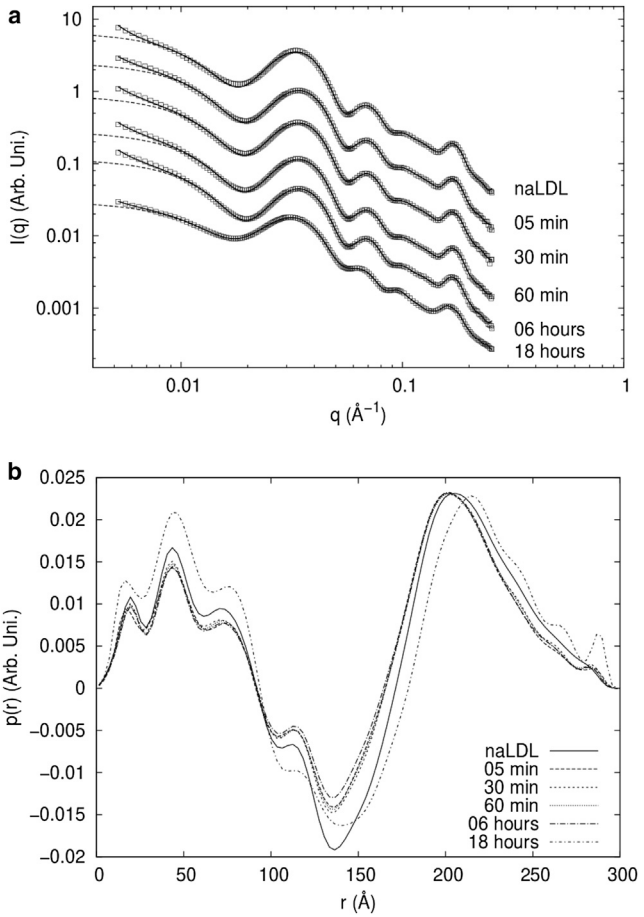

FIGURE 3 GIFT applied to LDL SAXS data. (*a*) Fitting (*solid curve*) of scattering data of LDL samples by the GIFT method. Also shown are the form factors (*dashed curves*) obtained from the decoupling procedure. (*b*) Pair distance distribution functions, $p(r)$, obtained with the GIFT method for LDL samples.

This maximum appears in the scattering data of all samples, but oxLDL-18 h has a broader maximum. These results show that the internal lamellar packing is preserved, at least partially, during the oxidation process.

The $p(r)$ curves obtained for the LDL particles show very similar features in the region between 0 and 300 Å for native LDL (naLDL) and oxLDL samples (Fig. 3 *b*). The maximum at ~200 Å is shifted to higher values in the oxLDL-18h sample, which might indicate changes in the electron density profile of LDL in this sample. The $p(r)$ curves obtained for the other oxLDL samples did not show clear differences when compared to the $p(r)$ from the naLDL sample.

Using the GIFT method, it is possible to obtain a good extrapolation for the form factor at angles lower than that given in the original experimental data. This is very important when using the deconvolution procedure to improve modeling stability. By using this to our knowledge new modeling method, it is possible to obtain a very good fit of the experimental data and calculate the electron density profile of the lipoproteins. To fit the form factor, we used a fixed anisotropy of 0.9, because LDL particles are known to be slightly oblate (42). The fixation of this parameter was necessary to improve the modeling stability, since anisotropy and size polydispersity can be correlated. The fitting parameters were the average radius, the size polydispersity, the constant background, and the scale factors. The radius of gyration of the Gaussian chain was determined for native LDL (naLDL) as 54 ± 5 Å, and this value was kept fixed for the other oxLDL samples. The fitting results can be seen in Fig. 4 *a* and the electron density profiles are shown in Fig. 4 *b*.

It is possible to observe several oscillations in the LDL electron density profile, which can be understood as variations on the electron density profile of the LDL particle. Interestingly, the positive-negative variation observed between ~100 and 140 Å, corresponds approximately to the length of phosphatidylcholine, the primary phospholipid in the LDL outer layer. This outer particle surface also has the presence of ApoB, which may slightly alter the height of these oscillations and probably is

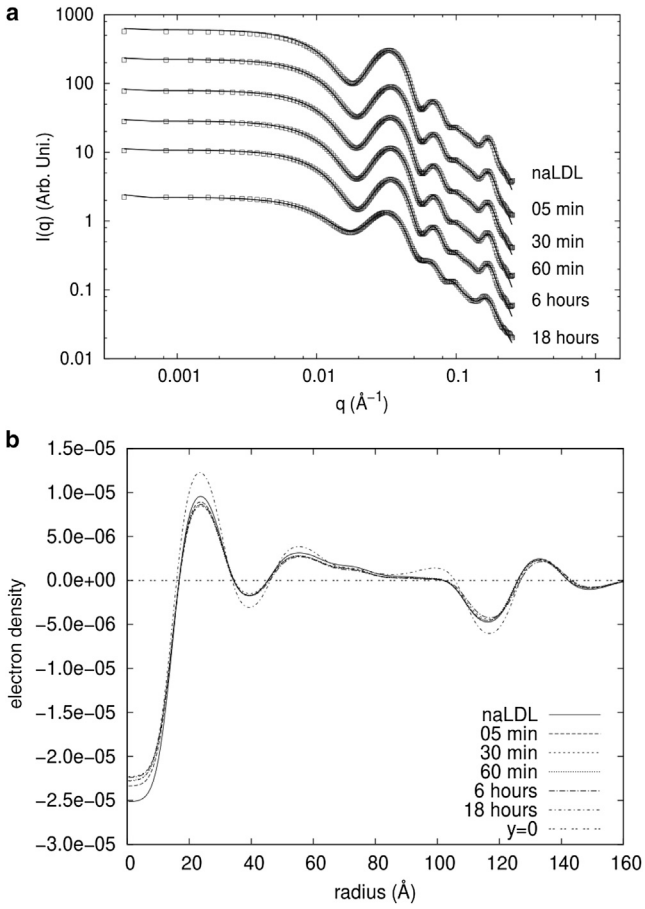

FIGURE 4 Deconvolution procedure applied to modeling of LDL SAXS data. (*a*) Form factor fitted with the deconvolution modeling procedure. Experimental data (*open squares*) and model fit (*solid lines*) are shown. (*b*) Electron density profiles of LDL samples obtained with the deconvolution modeling procedure.

responsible for the negative density that occurs for radius values >140 Å. For radius values <100 Å, it is possible to observe other systematic variations in the electron density profile that are related to the well-defined region (oriented) in the center of the particle. This large variation in electron density profile may be due to the existing lamellar organization within LDL particles, which is associated with the maximum correlation curves scattering at $q = 0.17$ Å^{-1}. It is noteworthy that the sample oxLDL-18h has a significantly different electron density profile when compared with less oxidized and native LDL profiles. This difference indicates changes in both the core region and the phospholipid layer on the 18-h-oxidized particles.

The parameters obtained by deconvolution are shown in Table 2. As can be seen, there was no evolution of the mean radius of particles as a function of sample oxidation time. Moreover, size polydispersity of LDL particles increased significantly for the oxLDL-18h sample. Taking into account that polydispersity is ~15 Å for all samples, the obtained particle sizes are consistent with those presented in the literature (27,41).

Interestingly, there is a significant change in the Debye scale factor (S_{C2} in Eq. 9) for the sample oxidized for 18 h (Table 2). This can be interpreted as an increase in the amount of flexible chains of ApoB exposed on the surface of LDL particles. This result is consistent with the idea that LDL oxidation occurs initially on the lipids and also at ApoB hydrophobic sites (43,44). These sites, initially immersed in the region of phospholipid carbon chains, become exposed when oxidized.

High-density lipoproteins

HDL samples did not show evidence of oligomerization, and therefore, it was not necessary to apply the GIFT method to retrieve the form factor. Fig. 5, *a* and *b*, shows the experimental scattering data fitted with the IFT method and the obtained $p(r)$ curves. As can be seen from the scattering intensity and corresponding $p(r)$ curves, the results with HDL are very different from those obtained with the LDL samples. This indicates that there are important structural differences between the two types of lipoprotein. From the results, one can see that the oxidation process in HDL induces small changes in the scattering intensities and $p(r)$ curves, indicating that no significant structural changes are induced by oxidation.

TABLE 2 Parameters obtained by the deconvolution modeling procedure for LDL samples

Sample	Radius (Å)	Polydispersity (Å)	S_{C2}
naLDL	155.7 ± 2.8	14.3 ± 0.4	0.19 ± 0.05
05 min	155.6 ± 1.0	14.34 ± 0.24	0.203 ± 0.008
30 min	156.1 ± 0.8	14.07 ± 0.22	0.206 ± 0.007
60 min	155.4 ± 1.0	14.11 ± 0.25	0.204 ± 0.008
06 hours	156.7 ± 1.1	14.42 ± 0.20	0.206 ± 0.008
18 hours	156.0 ± 2.8	15.8 ± 0.6	0.292 ± 0.018

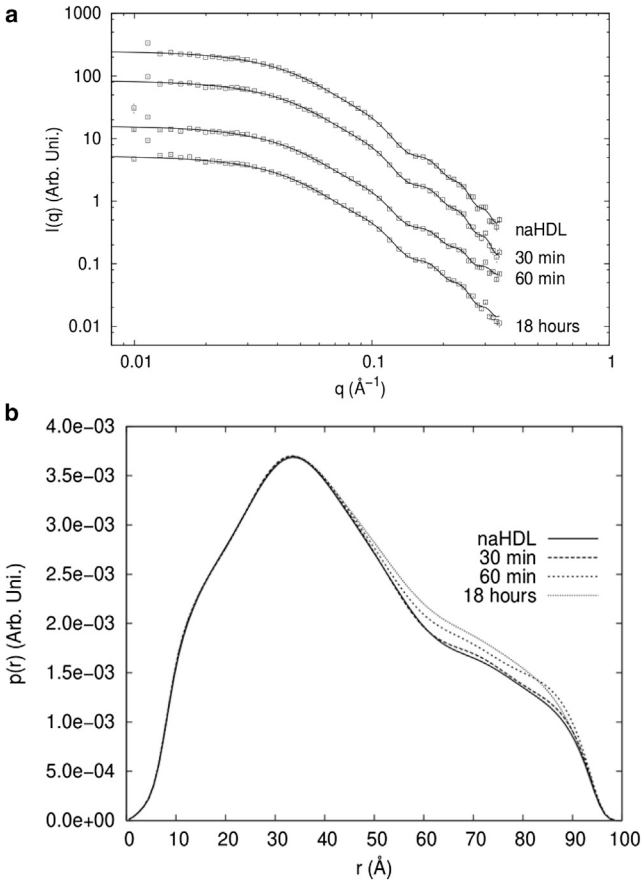

FIGURE 5 Indirect Fourier transform applied to HDL SAXS data. (*a*) HDL scattering intensity data fitted with the IFT method. Experimental data (*open squares*) and model fit (*solid lines*) are shown. (*b*) HDL pair distance distribution function curves, $p(r)$, obtained by the IFT method.

Fig. 6 *a* shows the experimental scattering data for HDL fitted with the deconvolution method. The results obtained with this method are shown in Table 3. Fitting results were obtained by fixing particle anisotropy at 1.0. This assumption was based on data from several studies in the literature that indicate that HDL particles are practically spherical. Also, similar to the LDL case, the fitting procedure is not stable if both anisotropy and polydispersity are optimized, since they make similar contributions to the scattering intensity. Another important aspect is that the contribution from a Gaussian chain was not important and always gave scale factors close to zero, with large uncertainty. Because of this, this parameter was not considered in the analysis procedure, and was fixed at zero. This is an interesting result and suggests that for HDL, the proteins should be located around the entire surface and not only in a particular region, as in the case of the LDL. Also, oxidation does not induce the appearance of floppy or flexible regions in the HDL structure.

HDL electron density profiles (Fig. 6 *b*) present a positive-negative variation between ~40 and 60 Å, which may correspond to the phospholipid monolayer region with the

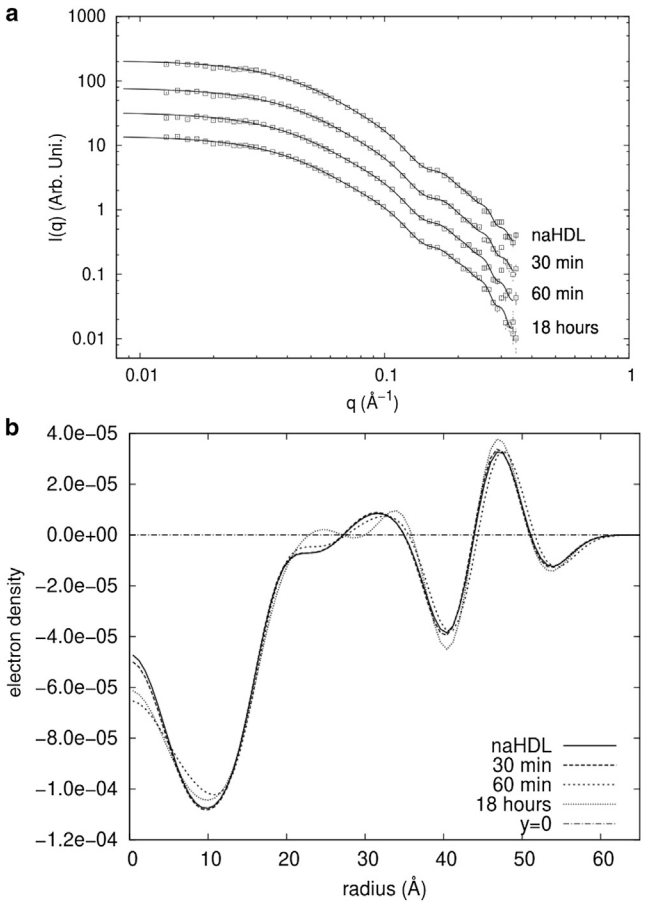

FIGURE 6 Deconvolution procedure applied to the modeling of LDL SAXS data. (*a*) HDL scattering intensity data fitted with the deconvolution modeling procedure. Experimental data (*open squares*) and model fit (*solid lines*) are shown. (*b*) Electron density profiles for HDL samples obtained with the deconvolution modeling procedure.

proteins immersed. This region does not vary between the different samples, suggesting that it is not affected by the oxidation of the samples. Likewise, all the curves converge to zero in the same radius value, indicating that the particle diameter does not change due to oxidation. Some small changes in the electron density profile are observed mainly below 30 Å and may be induced by oxidation effects.

The HDL electron density profiles have far fewer oscillations than those obtained for LDL samples, in agreement with the fact that these two lipoproteins have important structural and size differences. HDL particles have a less organized core than LDL particles and higher relative size polydispersity. In addition, the proteins that compose the two lipoprotein structures are very different. Although LDL particles have only ApoB, HDLs may contain serveral apolipoproteins, the amount varying from particle to particle (45). This variable number of proteins in HDL particles makes them intrinsically less monodisperse and with a less well defined structure compared to LDL particles. These peculiarities of HDL particles are reflected on the obtained electron density profiles and on the model results.

In any case, since it was not possible to observe any significant structural difference in HDL electron density profiles induced by copper oxidation, the SAXS results and modeling indicate that HDL particles are more resistant to copper oxidation than are LDL particles.

TABLE 3 Parameters obtained by the deconvolution modeling procedure for HDL samples

Sample	Radius (Å)	Polydispersity (Å)
naHDL	55 ± 6	8.5 ± 1.0
30 min	55 ± 3	8.3 ± 0.8
60 min	56 ± 7	8.7 ± 1.1
18 hours	55 ± 6	8.9 ± 1.0

DLS results

A comparison of the temporal autocorrelation curves of all LDL samples (Fig. S3 *a*) indicates that only the sample oxidized for 18 h shows a significant change. This difference is probably related to the increase in size polydispersity of the sample, which was also observed on the SAXS analyses. Fig. S3 *a* shows a slight variation in the temporal autocorrelation curve of oxLDL-6h as well. The experimental data and the fitting curve are slightly more visible from 300 μs and further.

It is possible to estimate the average diameter of the particles in each sample through the diameter distribution. The average diameter is taken as the maximum of the distribution and the uncertainty of each diameter as the width at two-thirds of the maximal high.

Experimental autocorrelation data from HDL samples can be seen in Fig. S3 *b*. The main information present in these curves is the appearance of clusters in the oxHDL-18h data, which is characterized by a slower decay compared to other autocorrelation curves. Although for naHDL and other oxidation curves the autocorrelation data reach (near) zero when $\tau = 100$ μs, the oxHDL-18h data reach (near) zero when $\tau = 400$ μs. These clusters have diameters estimated at 50 ± 17 nm, which may explain why they have not been observed in SAXS measurements, as the resolution of the experimental setup was ~70 nm. The obtained mean radius of each sample is presented in Table 4.

TABLE 4 Radius values obtained through DLS measurements

Sample	Mean diameter (nm)
naLDL	20 ± 6
oxLDL-05min	20 ± 6
oxLDL-30min	20 ± 6
oxLDL-60min	19 ± 6
oxLDL-6h	20 ± 6
oxLDL-18h	21 ± 7
naHDL	5.7 ± 2.3
oxHDL-30min	7.3 ± 2.5
oxHDL-60min	7.5 ± 2.9
oxHDL-18h	8 ± 4

ZS results

Typical results for normalized transmittance as a function of z-position of the sample are presented in Fig. 7 *a*. It can be observed that the peak-to-valley distance decreases with an increase in sample oxidation time. Through the fit to the experimental data using the thermal lens model (Eq. 1), we obtained the parameter θ of each sample, which is proportional to the peak-to-valley distance. Results show a decrease of θ as a function of sample oxidation time (Fig. 7 *b*). A similar behavior was observed with LDL particles (32,41). LDL samples stop presenting a nonlinear optical response ($\theta = 0$) at ~90 min of in vitro oxidation with copper, whereas HDL samples presented a nonlinear optical response (under the same experimental conditions) even after 18 h of in vitro oxidation time. This indicates that there are important differences between the two lipoprotein types in the oxidation process and also supports SAXS results indicating that HDL particles are more resistant to oxidation than LDL particles.

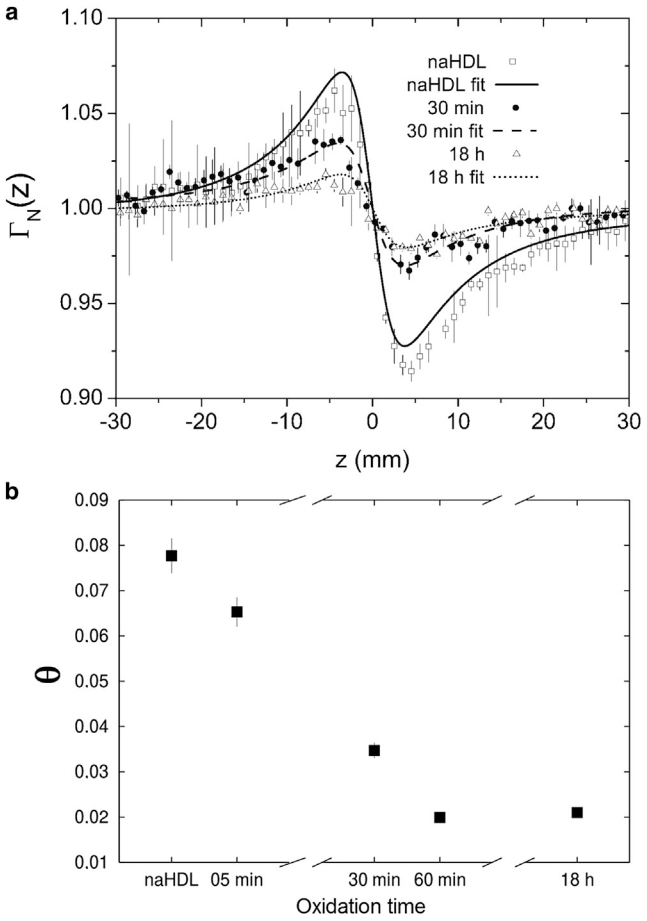

FIGURE 7 Results from ZS analysis. (*a*) Average nonlinear transmittance curves of naHDL, oxHDL-30min and oxHDL-18h. The solid and dashed lines are fits obtained with the thermal lens model. (*b*) θ parameter as a function of oxidation time for HDL samples, obtained with the thermal lens model.

DISCUSSION

The values of the average particle diameters for LDL and HDL samples obtained using the DLS and SAXS techniques show that oxidation process does not alter particle size. On the other hand, the SAXS data of LDL samples indicate that the size polydispersity of particles increases when the samples are subjected to long oxidation times (e.g., 18 h). Interestingly, in the case of HDL particles, there appeared to be no evidence of increased size polydispersity of particles as a function of sample oxidation time.

SAXS results also showed that LDL particles have a lamellar packing of cholesterol in their core. This organization remains, at least partially, even after 18 h of in vitro oxidation with copper ions. In contrast, SAXS curves of HDL showed no characteristic peak associated with repetition distance, which indicates that HDL particles have a disorganized lipid core.

LDL samples in the different stages of oxidation presented the formation of small aggregates, which could be modeled as volume fractal clusters by using the GIFT method of analysis. However, due to the limited experimental resolution, it was not possible to obtain a precise size for such clusters. Moreover, from the analysis of the HDL SAXS results (at least on the angular range covered in the experiments), no formation of aggregates or oligomers was observed. On the other hand, the DLS technique indicated that the oxHDL-18h sample showed formation of larger aggregates. However, since the fraction of such aggregates was very small, and since their size is near that of SAXS setup resolution, it was not possible to detect their influence on the SAXS data.

None of the LDL samples oxidized for up to 6 h showed any change in the intensity scattering data and electron density profile compared to the naLDL results. However the oxLDL-18h sample presented important differences: an increase of polydispersity, differences across the electron density profile, and an increase in the Gaussian chain scale factor. The increase of size polydispersity of particles on the sample oxidized for 18 h was also confirmed by the DLS data. Interestingly, for the oxLDL-18h, the electron density profile differs from that of the naLDL not only in the inner core, but also in the outer shell region of the particles (Fig. 4 *b*), which might indicate an important change over the complete structure of the lipoprotein. Finally, the observed increase in the Gaussian chain scale factor can be understood as an increase in the number of flexible or floppy regions on the protein sequence, which may indicate that somehow the oxidation is changing the protein structure, either by making it less structured or by causing some regions of the protein that were attached to the surface detach and become loose. All these results provide indications regarding the structural changes induced in the LDL particles due to the oxidation process. It is well known that oxidative modification of LDLs leads to loss of

recognition by the LDL receptor and a shift to recognition by scavenger receptors present in macrophages (10). Scavenger receptors are not downregulated in response to increased intracellular cholesterol and the accumulation of cholesterol leading to the development of foam cells, the hallmark of the artery lesion known as fatty streak. The failure in particle recognition by the system is related to the alteration of the protein structure. Therefore, oxidation induces changes in the ApoB constituent, making the particle unable to bind the LDL receptor (46). Such a change in protein structure was detected in the SAXS results, mainly by changes on the electron density profile and the Gaussian chain contribution. On the other hand, HDL samples showed no significant differences between native and oxidized samples, indicating that this kind of lipoprotein is more resistant to oxidation. This resistance to oxidation is due to the presence of several antioxidant enzymes associated with HDL particles, such as paraoxonase (47) and apolipoproteins (48).

The modeling strategy applied to the analysis of SAXS data, as well as use of the to our knowledge new deconvolution procedure, provided a unique way to study lipoproteins, permitting calculation of the electron density profile directly from the experimental SAXS data. In all the cases presented, we were able to obtain a very good fit to the experimental data.

It is interesting to compare the ZS results obtained with HDL and LDL particles. Since all lipoproteins present similarities in their overall structure, it is possible that the mechanism of thermal lens formation is also similar. The ZS experiments with HDL samples showed that the decrease of the θ parameter as a function of oxidation time occurs at a lower rate than observed for the LDL samples (32).Although LDL loses the nonlinear optical response signal altogether after <2 h of in vitro oxidation, HDL presents this signal for over 18 h. It has been shown previously in the case of LDL experiments that the behavior of the parameter θ is inversely proportional to the sample's thermal diffusivity (32). The thermal lens is formed because the sample absorbs heat from the Gaussian laser beam, which diffuses radially across it, imposing a temperature gradient. If the heat propagates slowly, it creates a variation of the refractive index through the radial direction, which gives rise to the lens formation. However, the more oxidized the LDL sample, the greater is the thermal diffusivity, and for samples oxidized for >90 min, the thermal lens does not form in the timescale of the experiment (milliseconds) (32). Recent studies have shown that the increase of thermal diffusivity is partially associated with the production of hydroperoxides during the oxidation process (32). From this picture, one can conclude that the changes in the ZS signal are related to a global modification in the sample as a function of the oxidation process, namely, to structural modifications and chemical reactions occurring in the solution, which form hydroperoxides. The SAXS results showed that when subjected to oxidation, HDL particles presented significantly fewer structural changes than did LDL particles. This information on the nanoscale can be directly correlated to ZS results, which provide information on a much larger length scale.

CONCLUSIONS

We have presented a controlled and systematic study of LDL and HDL structural changes due to in vitro oxidation of the samples with copper ions. SAXS, DLS, and ZS techniques were used to investigate and characterize the structure of the particles directly in solution. The SAXS data were analyzed using a to our knowledge new methodology capable of fitting the experimental scattering data and providing the corresponding electron density profile and other structural parameters. We conclude that compared to previous works using different modeling approaches, this to our knowledge new modeling approach provides much more reliable results and therefore seems to be more appropriate for the study of lipoproteins in solution. Also, the SAXS strategy for data analysis and modeling presented in this work can certainly be used as a guide for analyzing this kind of nanoparticle in solution. Results showed differences in the electron density profile both in the cholesterol core and in the phospholipid monolayer for samples oxidized for 18 h, compared to native particles. Furthermore, size polydispersity of oxLDL-18h increased, as did the scale factor of the Gaussian chain contribution. This term may be associated with changes (loss) in the overall symmetry of the particle, an increase in the flexible parts of the lipoprotein, which may indicate structural changes on the protein that embraces the lipoprotein, or some breakage of ApoB.

Our SAXS results with LDL samples show that the lamellar organization of cholesterol in the particle core remains at least partially structured even after 18 h of oxidation. All these results show that, despite the fact that LDL particles lose their biological function after an oxidation process as extensive as that generated by 18 h of incubation with copper, the overall structure of the lipoprotein is still similar to that of the native particle. This indicates that severe changes might occur in ApoB due to oxidation.

With respect to HDL, both optical and structural characterization results reveal that this particle presents a higher resistance to oxidation than do LDL particles. With the ZS technique, even after oxidation for 18 h, HDL samples continue to show a nonlinear optical signal distinguishable from the background. As in the case of LDL, oxidation of HDL particles shows a decrease of the amplitude of this signal as a function of oxidation time, but unlike the case for LDL, oxidation of HDL particles does not lead to a complete loss of signal. SAXS results did not show any drastic structural changes due to oxidation of HDL particles. The DLS technique showed a tendency in the oxHDL-18h

sample to form a small fraction of aggregates. All the structural investigations for the nanoparticles presented in this work indicated that LDL particles are more susceptible to oxidation than HDL particles.

SUPPORTING MATERIAL

Three figures are available at http://www.biophysj.org/biophysj/supplemental/S0006-3495(14)00469-X.

The authors thank Dennys Reis and Renata N. Bicev for their support on the DLS measurements. The authors acknowledge the Brazilian Synchrotron Light Laboratory (LNLS) for SAXS data acquisition (project num. SAXS1 - 10713).

This study was supported by The National Counsel for Scientific and Technological Development (CNPq), São Paulo Research Foundation (FAPESP), and the National Institute of Science and Technology of Complex Fluids (INCT-FCx).

REFERENCES

1. Dominiczak, M. H., and M. J. Caslake. 2011. Apolipoproteins: metabolic role and clinical biochemistry applications. *Ann. Clin. Biochem.* 48:498–515.
2. Harris, J. R., S. Lund-Katz, and M. Phillips. 2010. High density lipoprotein structure–function and role in reverse cholesterol transport. *In* Cholesterol Binding and Cholesterol Transport Proteins Springer, Dordrecht, The Netherlands, pp. 183–227.
3. Esterbauer, H., J. Gebicki, …, G. Jürgens. 1992. The role of lipid peroxidation and antioxidants in oxidative modification of LDL. *Free Radic. Biol. Med.* 13:341–390.
4. Zhang, Y., I. Zanotti, …, D. J. Rader. 2003. Overexpression of apolipoprotein A-I promotes reverse transport of cholesterol from macrophages to feces in vivo. *Circulation.* 108:661–663.
5. Movva, R., and D. J. Rader. 2008. Laboratory assessment of HDL heterogeneity and function. *Clin. Chem.* 54:788–800.
6. Superko, H. R. 2009. Advanced lipoprotein testing and subfractionation are clinically useful. *Circulation.* 119:2383–2395.
7. Badimon, L., R. F. Storey, and G. Vilahur. 2011. Update on lipids, inflammation and atherothrombosis. *Thromb. Haemost.* 105 (*Suppl 1*):S34–S42.
8. Mahdy Ali, K., A. Wonnerth, …, J. Wojta. 2012. Cardiovascular disease risk reduction by raising HDL cholesterol—current therapies and future opportunities. *Br. J. Pharmacol.* 167:1177–1194.
9. Yoshida, H., and R. Kisugi. 2010. Mechanisms of LDL oxidation. *Clin. Chim. Acta.* 411:1875–1882.
10. Yu, X.-H., Y.-C. Fu, …, C.-K. Tang. 2013. Foam cells in atherosclerosis. *Clin. Chim. Acta.* 424:245–252.
11. Viswambharan, H., X. F. Ming, …, Z. Yang. 2004. Reconstituted high-density lipoprotein inhibits thrombin-induced endothelial tissue factor expression through inhibition of RhoA and stimulation of phosphatidylinositol 3-kinase but not Akt/endothelial nitric oxide synthase. *Circ. Res.* 94:918–925.
12. Navab, M., S. Y. Hama, …, A. M. Fogelman. 2000. Normal high density lipoprotein inhibits three steps in the formation of mildly oxidized low density lipoprotein: step 1. *J. Lipid Res.* 41:1481–1494.
13. Navab, M., J. A. Berliner, …, A. M. Fogelman. 2001. HDL and the inflammatory response induced by LDL-derived oxidized phospholipids. *Arterioscler. Thromb. Vasc. Biol.* 21:481–488.
14. Navab, M., G. M. Ananthramaiah, …, A. M. Fogelman. 2004. The oxidation hypothesis of atherogenesis: the role of oxidized phospholipids and HDL. *J. Lipid Res.* 45:993–1007.
15. Gómez, S. L., R. F. Turchiello, …, A. M. F. Neto. 2004. Characterization of native and oxidized human low-density lipoproteins by the Z-scan technique. *Chem. Phys. Lipids.* 132:185–195.
16. Monteiro, A. M., M. A. N. Jardini, …, M. Gidlund. 2009. Cardiovascular disease parameters in periodontitis. *J. Periodontol.* 80:378–388.
17. Monteiro, A. M., M. A. N. Jardini, …, M. Gidlund. 2012. Measurement of the nonlinear optical response of low-density lipoprotein solutions from patients with periodontitis before and after periodontal treatment: evaluation of cardiovascular risk markers. *J. Biomed. Opt.* 17:115004.
18. Laggner, P., K. Müller, …, A. Holasek. 1973. Studies on the structure of lipoprotein A of human high density lipoprotein HDL3: the spherically averaged electron density distribution. *FEBS Lett.* 33:77–80.
19. Atkinson, D. D., R. J. Deckelbaum, …, G. G. Shipley. 1977. Structure of human plasma low-density lipoproteins: molecular organization of the central core. *Proc. Natl. Acad. Sci.* 74:1042–1046.
20. Laggner, P., K. Müller, and O. Kratky. 1976. X-ray small angle scattering on human plasma lipoproteins. *J. Colloid Interface Sci.* 55:102–108.
21. Glatter, O. 1981. Convolution square root of band-limited symmetrical functions and its application to small-angle scattering data. *J. Appl. Crystallogr.* 14:101–108.
22. Glatter, O., and B. Hainisch. 1984. Improvements in real-space deconvolution of small-angle scattering data. *J. Appl. Crystallogr.* 17:435–441.
23. Meyer, D. F., A. S. Nealis, …, S. J. Perkins. 1996. Time-course studies by synchrotron x-ray solution scattering of the structure of human low-density lipoprotein during Cu^{2+}-induced oxidation in relation to changes in lipid composition. *Biochem. J.* 319:217–227.
24. Liu, Y., D. Luo, and D. Atkinson. 2011. Human LDL core cholesterol ester packing: three-dimensional image reconstruction and SAXS simulation studies. *J. Lipid Res.* 52:256–262.
25. Prassl, R. 2011. Human low density lipoprotein: the mystery of core lipid packing. *J. Lipid Res.* 52:187–188.
26. Prassl, R., and P. Laggner. 2009. Molecular structure of low density lipoprotein: current status and future challenges. *Eur. Biophys. J.* 38:145–158.
27. Ren, G., G. Rudenko, …, H. J. Pownall. 2010. Model of human low-density lipoprotein and bound receptor based on cryoEM. *Proc. Natl. Acad. Sci. USA.* 107:1059–1064.
28. Oliveira, C. L. P., B. B. Gerbelli, …, J. S. Pedersen. 2012. Gaussian deconvolution: a useful method for a form-free modeling of scattering data from mono- and multilayered planar systems. *J. Appl. Crystallogr.* 45:1278–1286.
29. Havel, R. J., H. A. Eder, and J. H. Bragdon. 1955. The distribution and chemical composition of ultracentrifugally separated lipoproteins in human serum. *J. Clin. Invest.* 34:1345–1353.
30. Fernvik, E. C., D. F. Ketelhuth, …, M. Gidlund. 2004. The autoantibody repertoire against copper- or macrophage-modified LDL differs in normolipidemics and hypercholesterolemic patients. *J. Clin. Immunol.* 24:170–176.
31. Carter, C. A., and J. M. Harris. 1984. Comparison of models describing the thermal lens effect. *Appl. Opt.* 23:476–481.
32. Santos, P. R., T. C. Genaro-Mattos, …, A. M. Figueiredo Neto. 2012. Behavior of the thermal diffusivity of native and oxidized human low-density lipoprotein solutions studied by the Z-scan technique. *J. Biomed. Opt.* 17:105003.
33. Kellermann, G., F. Vicentin, …, I. Torriani. 1997. The small-angle x-ray scattering beamline of the Brazilian Synchrotron Light Laboratory. *J. Appl. Crystallogr.* 30:880–883.
34. Hammersley, A. P., S. O. Svensson, …, D. Hausermann. 1996. Two-dimensional detector software: from real detector to idealised image or two-theta scan. *High Press. Res.* 14:235–248.
35. Glatter, O. 1977. A new method for the evaluation of small-angle scattering data. *J. Appl. Crystallogr.* 10:415–421.
36. Oliveira, C. L. P., M. A. Behrens, …, J. S. Pedersen. 2009. A SAXS study of glucagon fibrillation. *J. Mol. Biol.* 387:147–161.

37. Pedersen, J. S., S. Hansen, and R. Bauer. 1994. The aggregation behavior of zinc-free insulin studied by small-angle neutron scattering. *Eur. Biophys. J.* 22:379–389.

38. Pedersen, J. S., and I. W. Hamley. 1994. Analysis of neutron and x-ray reflectivity data. 2. Constrained least-squares methods. *J. Appl. Crystallogr.* 27:36–49.

39. Provencher, S. W. 1982. CONTIN: a general-purpose constrained regularization program for inverting noisy linear algebraic and integral equations. *Comput. Phys. Commun.* 27:229–242.

40. Teixeira, J. 1988. Small-angle scattering by fractal systems. *J. Appl. Crystallogr.* 21:781–785.

41. Gómez, S. L., A. M. Monteiro, …, A. M. F. Neto. 2010. Cu and Fe metallic ions-mediated oxidation of low-density lipoproteins studied by NMR, TEM and Z-scan technique. *Chem. Phys. Lipids.* 163:545–551.

42. Orlova, E. V., M. B. Sherman, …, A. M. Gotto, Jr. 1999. Three-dimensional structure of low density lipoproteins by electron cryomicroscopy. *Proc. Natl. Acad. Sci. USA.* 96:8420–8425.

43. Singh, S., R. Suri, and C. G. Agrawal. 1995. Fluorescence properties of oxidised human plasma low-density lipoproteins. *Biochim. Biophys. Acta.* 1254:135–139.

44. Prassl, R., B. Schuster, …, M. J. Chapman. 1998. Thermal stability of apolipoprotein B100 in low-density lipoprotein is disrupted at early stages of oxidation while neutral lipid core organization is conserved. *Biochemistry.* 37:938–944.

45. Eisenberg, S. 1983. Lipoproteins and lipoprotein metabolism. A dynamic evaluation of the plasma fat transport system. *Klin. Wochenschr.* 61:119–132.

46. Steinberg, D. 2002. Atherogenesis in perspective: hypercholesterolemia and inflammation as partners in crime. *Nat. Med.* 8:1211–1217.

47. Durrington, P. N., B. Mackness, and M. I. Mackness. 2001. Paraoxonase and atherosclerosis. *Arterioscler. Thromb. Vasc. Biol.* 21:473–480.

48. Kontush, A., S. Chantepie, and M. J. Chapman. 2003. Small, dense HDL particles exert potent protection of atherogenic LDL against oxidative stress. *Arterioscler. Thromb. Vasc. Biol.* 23:1881–1888.

Supporting Material

Effect of oxidation on the structure of human low and high density human lipoproteins

Cristiano L. P. Oliveira, Priscila R. Santos, Andrea M. Monteiro and Antonio M. Figueiredo Neto

Instituto de Física, Universidade de São Paulo, São Paulo, Brazil

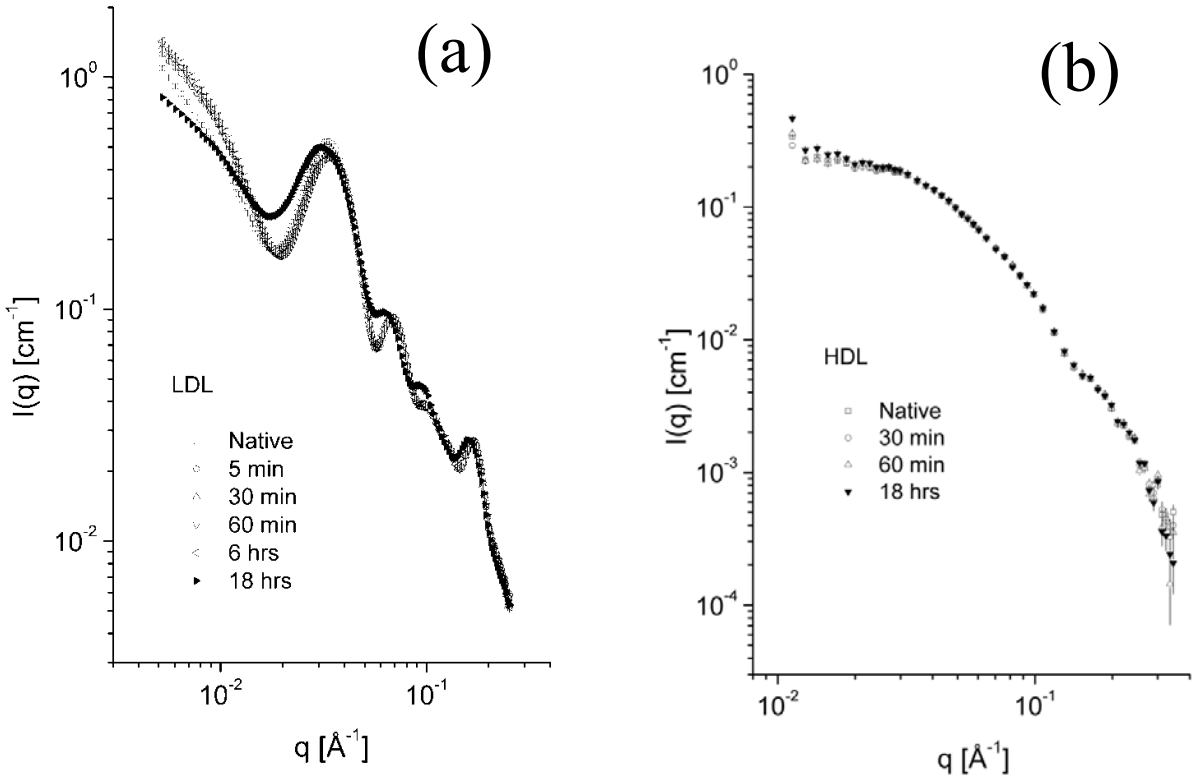

Figure S1: Experimental SAXS data for the studied lipoproteins. a) LDL scattering intensity data. b) HDL scattering intensity data.

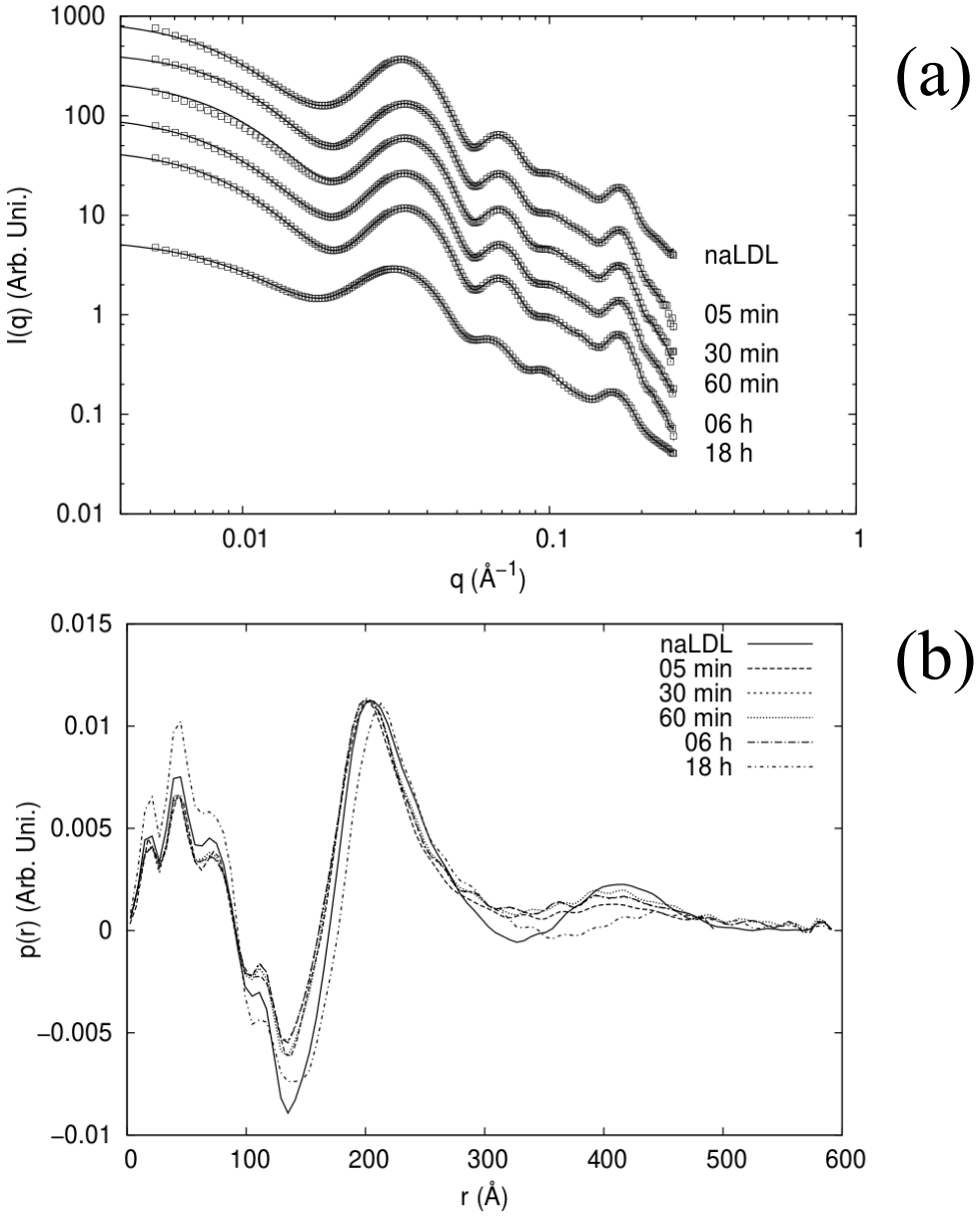

Figure S2: Indirect Fourier Transformation analysis for SAXS data from LDL samples. a) LDL scattering intensity data fitted with IFT method. Experimental data (open squares) and model fit (solid lines). b) LDL pair distances distribution function curves, p(r), obtained by the IFT method.

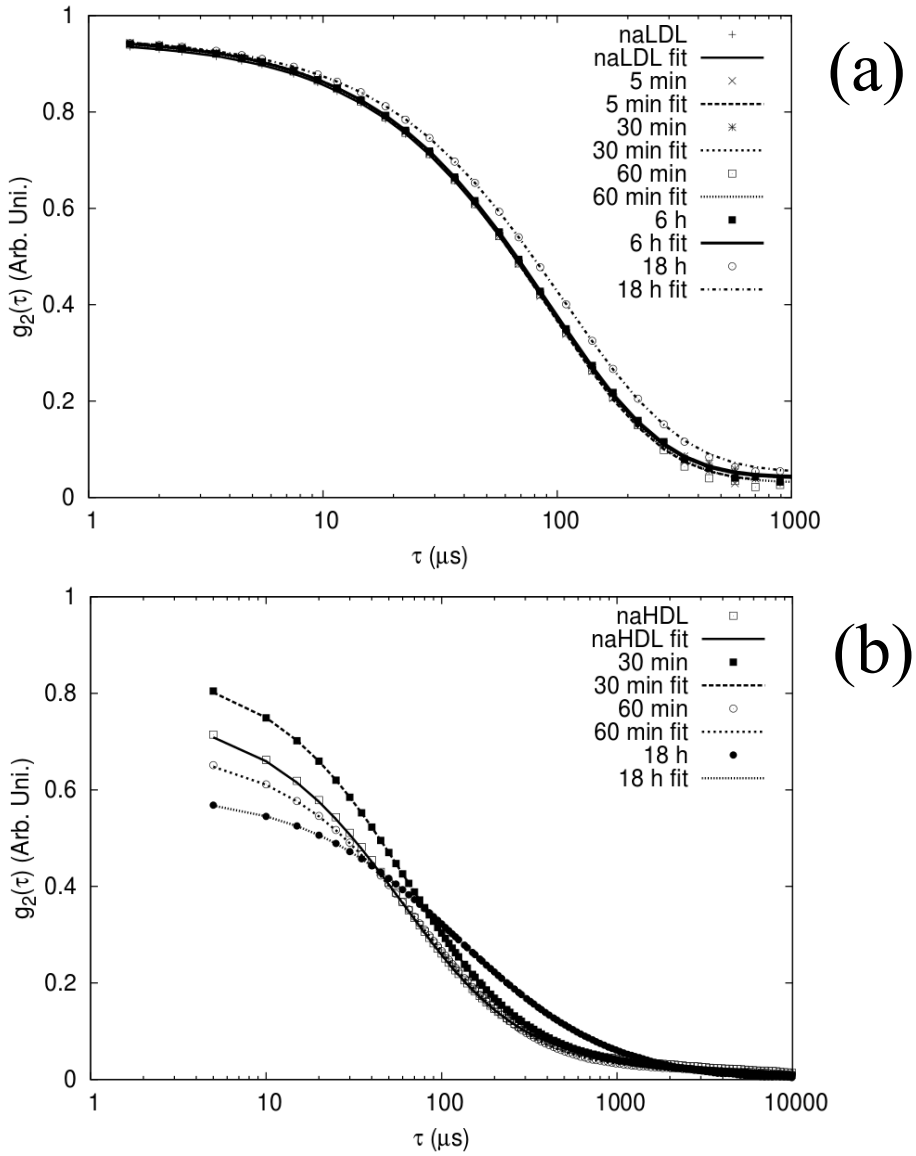

Figure S3: DLS results for LDL and HDL samples. a) DLS experimental autocorrelation curves and respectively fits for native and oxidized LDL samples. b) DLS experimental autocorrelation curves and respectively fits of native and oxidized HDL samples.